Chest Wall Disorders

7

Francesco Feletti, Bruna Malta, and Andrea Aliverti

7.1 Introduction

7.1.1 Study Techniques

The use of thoracic ultrasound (TUS) is becoming increasingly popular in the study of the chest wall and its alterations to both the soft tissue and skeletal components [1].

With an average thickness of 27 (±5) mm [2], the chest wall must be studied sonographically with medium-high (5–10 MHz) to high (>10 MHz) frequency transducers [1].

However, to cope with the limited penetration capacity and the restricted field of view of linear probes, it may be helpful to use convex transducers with frequencies between 3.5 and 5 MHz [3], especially in the case of extensive lesions or when the fat layer is particularly represented.

In certain cases, to ensure more reliable results, comparative evaluations of the same scans on both sides of the thorax can be useful.

7.1.2 Normal Finds

To locate pathological findings, it is imperative to recognize the natural appearance of the different chest wall components.

In an intercostal scanning, along the direction of the costal arches, underneath the thin echogenic layer of the skin, there is a subcutaneous connective tissue that shows highly variable echogenicity depending on the fat content and the degree of hydration.

Deep to the skin, the superficial fascia appears as a subtle echogenic line that delimits the muscular planes above.

The chest wall muscles, which present a streaked structure (echogenicity typical of skeletal muscle), have a variable thickness in different regions of the chest.

Electronic Supplementary Material The online version of this chapter (https://doi.org/10.1007/978-3-319-93055-8_7) contains supplementary material, which is available to authorized users.

F. Feletti (✉)
Dipartimento di Diagnostica per Immagini, Ausl della Romagna, Ospedale S. Maria delle Croci, Ravenna, Italy

Dipartimento di Elettronica, Informazione e Bioingegneria, Politecnico di Milano, Milan, Italy
e-mail: francesco.feletti@auslromagna.it

B. Malta
Dipartimento di Diagnostica per Immagini, Ausl di Ferrara, Ospedale Universitario di Ferrara, Ferrara, Italy
e-mail: mltbrn@unife.it

A. Aliverti
Dipartimento di Elettronica, Informazione e Bioingegneria, Politecnico di Milano, Milan, Italy
e-mail: andrea.aliverti@polimi.it

F. Feletti et al. (eds.), *Thoracic Ultrasound and Integrated Imaging*,
https://doi.org/10.1007/978-3-319-93055-8_7

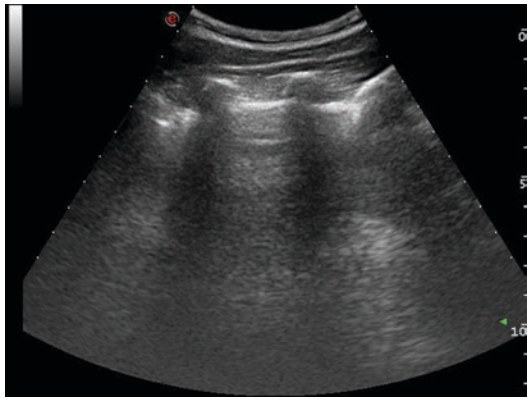

Fig. 7.1 Bat sign. *Bat sign* is the eponym used to describe the intercostal space transversally sounded, because the upper margin of the ribs resembles the wings of a bat seen in front, while the interposed pleural line represents the body

Deep to the chest wall muscles, in lean subjects, it is possible to identify the endothoracic fascia. It looks like an echogenic line, separated from the pleura only by a thin echogenic layer of fat tissue.

By rotating the probe perpendicularly to the ribs, the intercostal soft tissues are seen between two transversally scanned ribs (Fig. 7.1).

Typically, the bone structure of the thoracic cage partially reflects and partially absorbs ultrasounds, generating coarse rear shadow cones.

Costal acoustic shadows should be considered as standard criteria to be referred to; they are not present in subcutaneous emphysema because the air trapped in soft tissues masks the costal plane.

Instead, less intense and crisp costal shadows mean an increase in bone permeability to ultrasounds, and this may be due to an osteolytic lesion.

Therefore, every time costal shadows are less evident or abnormal, an X-ray examination is required.

7.2 Main Indications of Method

Thoracic ultrasound allows detailed and straightforward visualization of chest wall soft tissue alterations which, unlike in chest X-rays, may not be visible at all or may only result in minimal signs that are difficult to identify and interpret.

TUS is also sensitive enough to detect changes in the skeletal component, including costal fractures.

For these reasons, apart from diagnostic possibilities, the nonuse of ionizing radiation, rapidity of execution, availability, and low cost, TUS can be used alongside clinical examination and traditional radiology, especially in chest pain and in the study of any palpable swelling of the thoracic wall.

7.2.1 Chest Pain

While the visceral pleura and the lungs are insensitive to painful stimuli, thoracic pain is mediated by nerve fibres of the chest wall and the parietal pleura. Both the chest wall and the pleura are easily evaluated by TUS.

Therefore, TUS, along with clinical examination, can quickly exclude some of the most common causes of chest pain (Table 7.1), allowing for more rational use of traditional radiology and CT, with consequent benefits in diagnostic, radioprotection, and economic terms.

7.2.2 Studying Palpable Thoracic Wall Alterations

Thoracic ultrasound is often used as an initial examination when studying thoracic wall swelling.

Depending on the case, TUS may be the starting point or an intermediate step of the diagnostic process, which is useful for indicating other examinations or confirming a diagnosis that is already hypothesized based on anamnesis and the overall clinical picture.

Many of the conditions discussed below appear clinically as palpable masses.

7.2.3 Limitations

The main limitations of the chest wall ultrasound study are preexisting conditions which inhibit penetration of the ultrasound waves or hinder

Table 7.1 Most common causes of chest pain (underlined the causes that may give signs to TUS) [4] ECG: electrocardiogram; CTPA: computed tomography pulmonary angiography; CT: computed tomography.

Chest wall disorders	Possible ultrasound signs
Costal fractures	Lighthouse phenomenon (Fig. 7.2) Cortical interruption Bone fragments
Hematoma	<24 h isoechogenic or hyperechogenic collection with fine and dense echoes >24/<72 h hypo-anechogenic collection >72 h complex structure training
Neoplastic invasion of the chest wall	Echopermeability of bone components Infiltrating hypoechoic mass Local tissue softening
Chest wall abscesses	Complex structures, sometimes with gas bubbles
Pleurisy	Pleural line interruption Subpleural infiltrates Possible pleural effusion
Pleural empyema	Sometimes corpuscular pleural effusion
Pneumothorax	No gliding sign Presence of A lines
Lung diseases	
Pneumonia	Liver hepatitis, aerial bronchogram, hypervascularization, pleural effusion, B lines
Pulmonary embolism	Possible subpleural hypoecogens Pleural effusion. Diagnosis requires laboratory examinations and possibly angiopneumo CT
Mediastinal pathologies	
Acute aortic dissection	Expanded aorta with interspaced flaps in suprasternal or parasternal scans
Myocardial infarction	Normal TUS; diagnosis requires ECG and laboratory tests; possible role of echocardiography
Pericarditis	There may be a small pericardial effusion Diagnosis requires ECG
Esophageal breakage	TUS is not informative Diagnosis by X-ray or CT

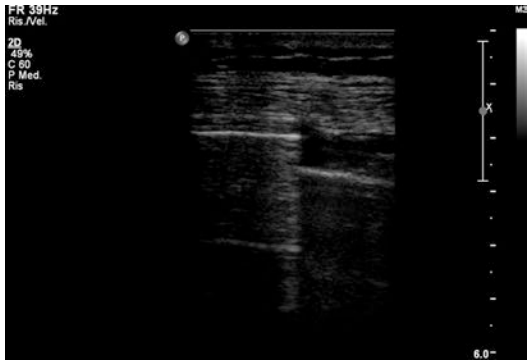

Fig. 7.2 Lighthouse phenomenon. The *lighthouse phenomenon* is a reverberation artifact that is generated between bone fragments in costal fractures

proper positioning of the probe such as subcutaneous emphysema, scarring or skin lesions, and external devices applied to the chest as electrodes or surgical dressings [5].

7.3 Soft Tissue Pathology

7.3.1 Hematomas

The sonographic appearance of hematomas changes over time.

In the acute phase (within 12–24 h of trauma), chest wall hematomas generate small, intense,

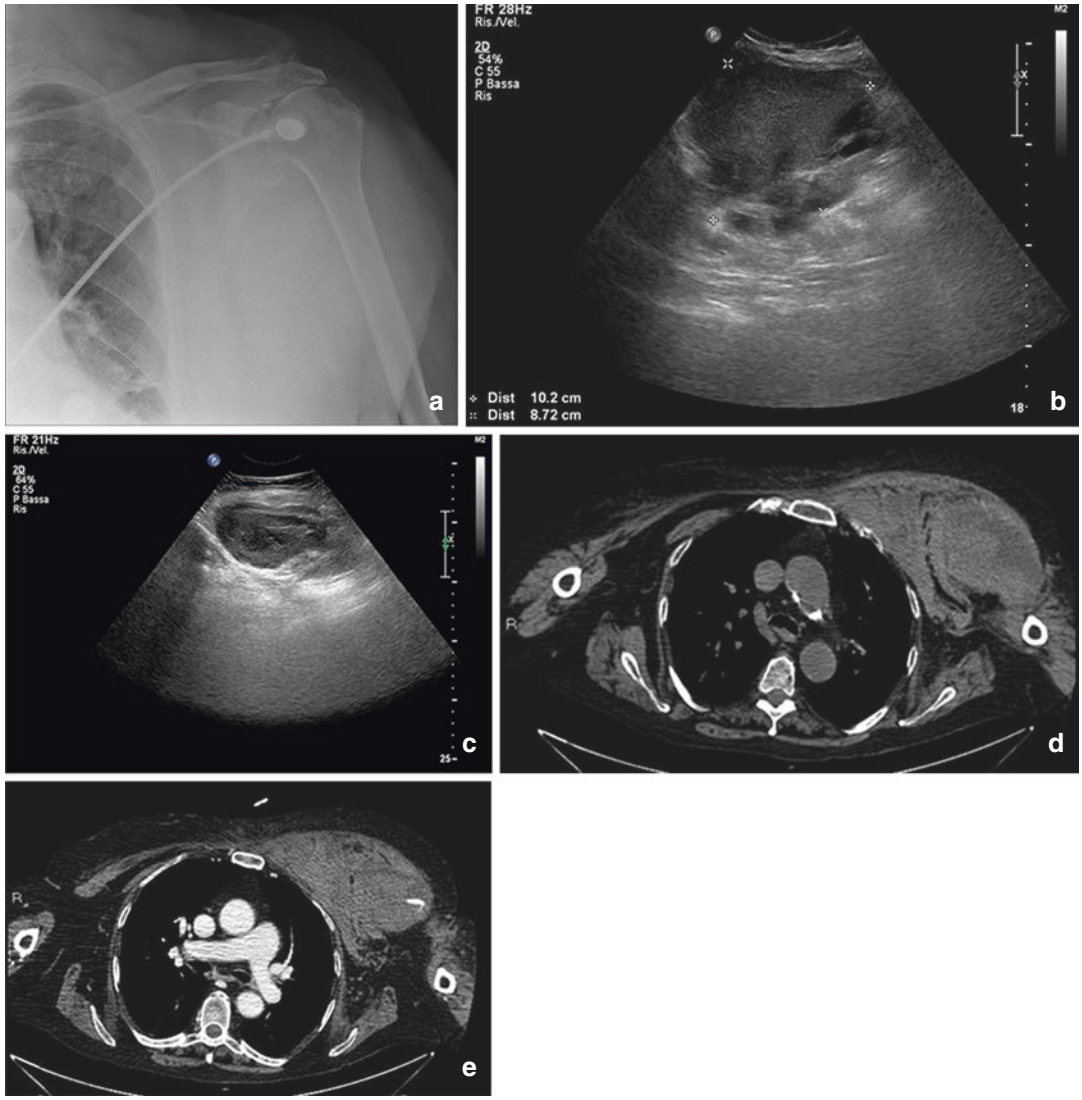

Fig. 7.3 Pectoral hematoma. The X-ray showed a soft tissue thickening (**a**). TUS (**b**, **c**) showed a complex echostructure formation that, together with the case history, allowed the diagnosis of a hematoma. The CT (**d**, **e**), on the other hand, made it possible to determine the anatomical relationships with the surrounding structures and to identify an active blood spill

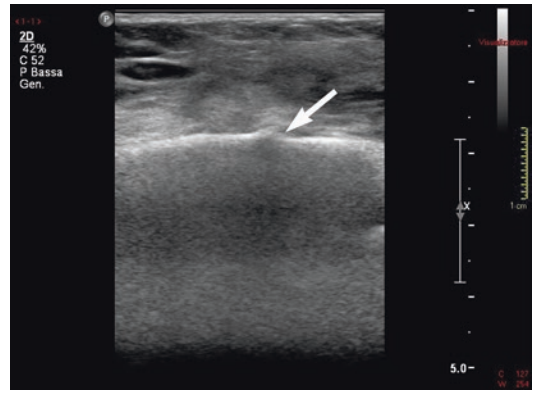

Fig. 7.4 Hemorrhagic effusion in the presence of a costal fracture (arrow). The hematoma appeared as shaded hyperechogenicity which made the interfaces between the muscular planes of the thoracic wall less evident

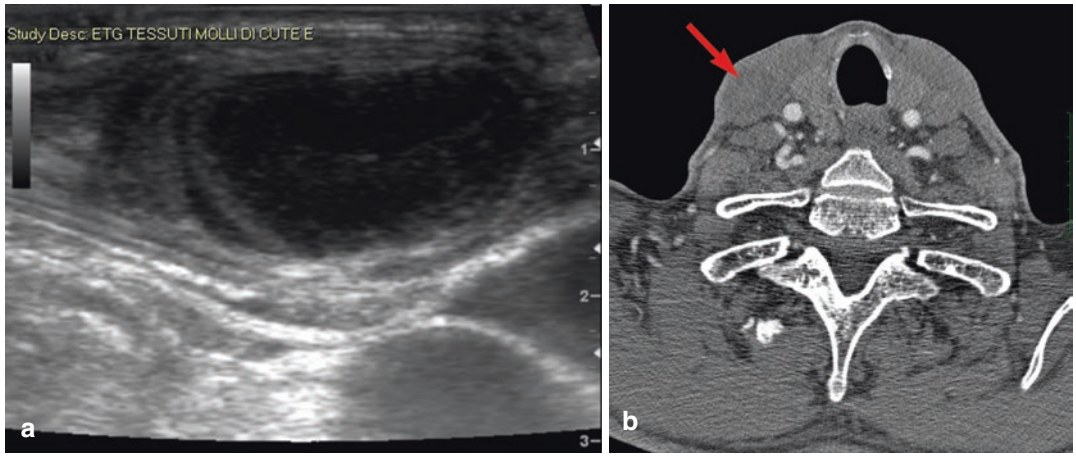

Fig. 7.5 Hematoma of the sternocleidomastoid muscle. The swelling at the base of the neck was evident in the ultrasound and showed an uneven appearance (**a**). A CT-angiography was then conducted to exclude active bleeding; the lesion was visible with the CT (**b**), although it was poorly delimited (arrow) due to the limited resolution of tissue contrast offered by this method, decidedly lower than the TUS, and there were no visible contrast spillages

uniform, and dense echo signals (Figs. 7.3a–e; and 7.4, Video 7.1).

Subsequently, following the lysis of red blood cells, they assume the appearance of hypoanechoic collections, sometimes uneven, due to the persistence of clots in the context (Fig. 7.5a, b).

Subsequently, smaller hematomas are reabsorbed.

Instead, larger ones are organized and have a complex structure with predominantly liquid contents.

At this stage, hematomas have an oval or melted shape with rounded edges and the echogenic wall may be thinner or thicker.

7.3.2 Cellulitis and Abscesses

Typically, cellulitis has a cobblestone appearance, while abscesses are complex structures with inhomogeneous intensity, size, and distribution of echoes [7] (Fig. 7.6a–c).

Usually, the echo layout within a lesion does not change with decubitus changes; this aspect, however, is not always easy to evaluate.

The abscess enters differential diagnosis with hematoma. However, a hematoma may become infected and become secondary into an abscess. As a result, the ultrasound data must always be complemented by anamnesis, objective examination, and laboratory findings (Fig. 7.7a–c).

7.3.3 Seroma

Seromas are free or partially organized posttraumatic or postsurgical lymphatic groups, while lymph cysts are congested, lymphatic vessels dilated upstream from an obstruction.

Both seroma and lymphatic cysts appear as anechoic, more or less elongated structures, with lateral acoustic shadows and back reinforcement (Fig. 7.8).

When studying a seroma group of the chest wall, it is essential to measure it and locate it with respect to the pleura, both to understand its origin and to address any ultrasound-guided interventional or surgical procedures.

7.3.4 Primary Expansion Processes

Tumours that originate from the chest wall are most often of mesenchymal origin. There are also several tumorlike masses which originate from the soft tissues of the chest wall.

Along with TUS, it is useful to evaluate the anatomical relationships of these expansive

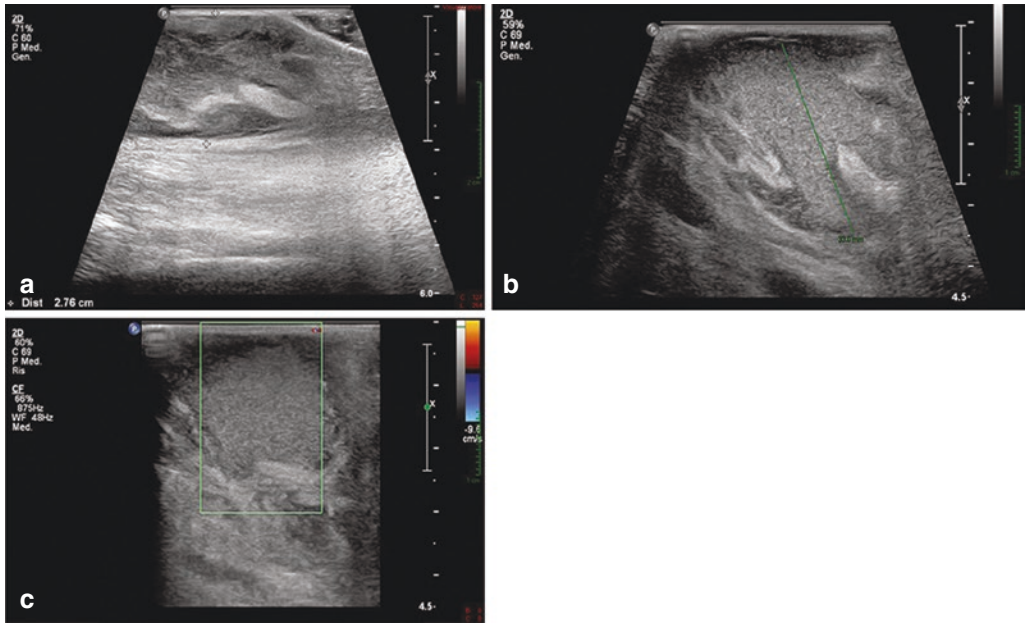

Fig. 7.6 Right subcutaneous dorsal abscess in a 38-year-old diabetic male patient. Ultrasound examination (**a**, **b**, **c**) revealed a complex mass of about 3 cm in the axillary region. The formation was hyperechogenic and characterized by thin, thickly crammed echoes

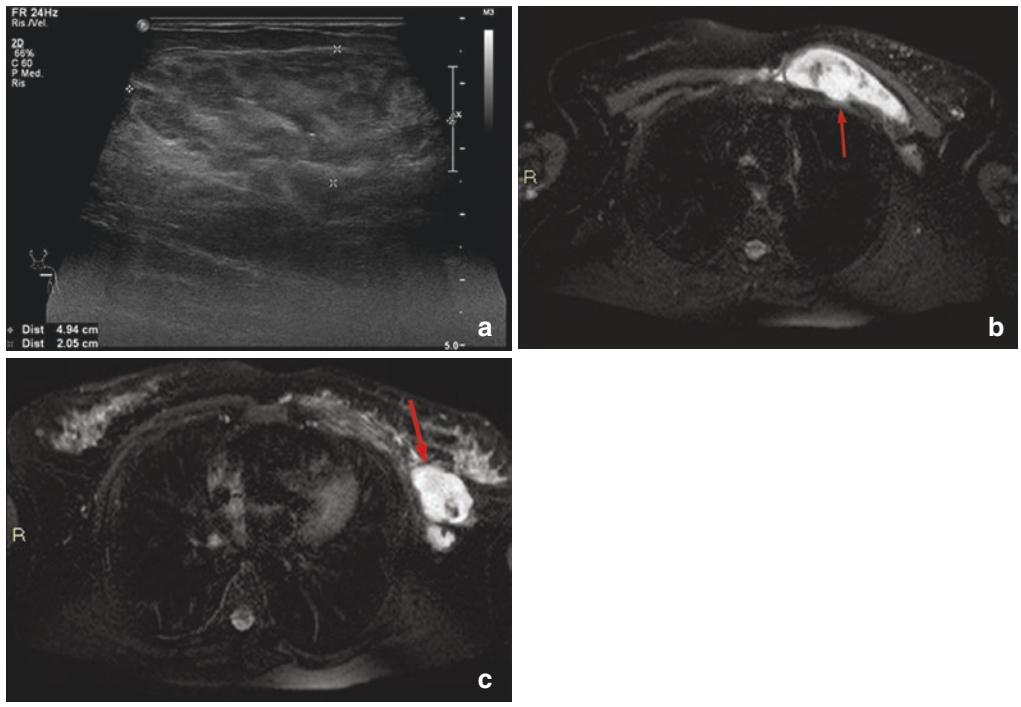

Fig. 7.7 Abscess of the chest wall. The ultrasound examination (**a**) showed the presence of a complex mass of about 5 cm in the left subclavian space. Echostructural characteristics alone did not allow for differential diagnosis from a hematoma. The MRI (**b**, **c**) showed the subfascial seat and extension to the axilla. The hyperintense aspect on T2w sequences and hypointense on T1w sequences were characterized by minute hypointense elements more evident in T1w sequences, which were attributed to a gas component. Contrast impregnation was poor and peripheral. The findings have been referred to as confluent abscessual collections

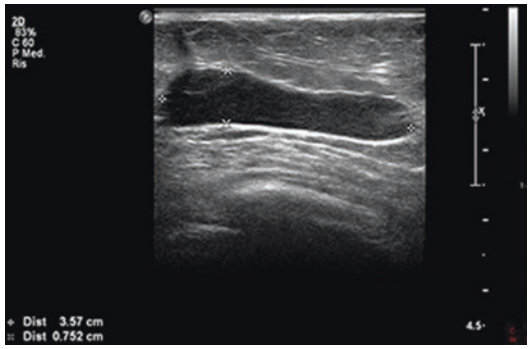

Fig. 7.8 Dysontogenetic lymphatic cyst. Soft tissue subcutaneous cyst in the left mammary site in a 5-year-old child. This formation was present from birth

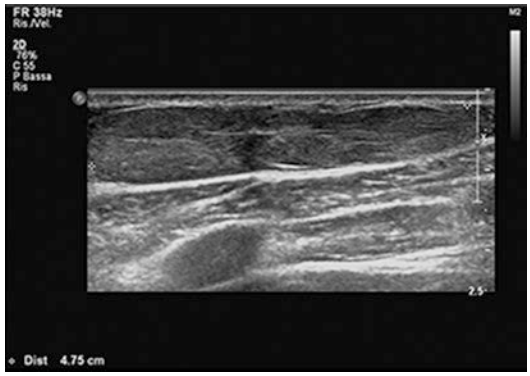

Fig. 7.9 Suprafascial lipoma of the right lateral thoracic wall. TUS showed the hyperechoic mass with regular margins and homogeneous echostructure of about 5 cm

processes with the pleura to confirm the extrathoracic origin of the lesion.

The pleura creates a cleavage plane and a natural barrier to the extension of the tumours and can be compressed and dislocated while the lung is not generally involved.

Therefore, even when they protrude in the chest cavity, these lesions retain obtuse joints with the chest wall.

7.3.5 Lipoma and fibrolipoma

Lipomas are the most common benign tumours in the chest wall, found both on the surface and at greater depths; deep lipomas are less frequent and generally larger.

Surface lipomas (Fig. 7.9) are found in the subcutaneous and are palpable. They are disk-shaped with a greater diameter parallel to the skin surface, compressible, and partially movable on the underlying planes.

Deep forms are intramuscular or intrafascial (Fig. 7.10a–e) and have varied, sometimes bizarre, shapes [7].

Sometimes large lipomas can widen an intercostal space or cause costal erosions through compression.

Finally, lipomatosis of the thoracic wall is a relatively rare condition characterized by multiple lipomas spread along the thoracic wall.

Regardless of location, lipomas have smooth, well-defined margins, poor internal structure, and uniform echogenicity, without signals at colour Doppler imaging (Fig. 7.11a–c).

Often lipomas contain intralesional fibrotic lines along the major axis of the lesion, that give them a streaked appearance.

As a result of traumas or inflammation, adiponecrosis may render the interior architecture less orderly, with hypo-anechoic areas and sometimes with small calcifications.

Fibroma and fibrolipoma have been frequently reported as benign tumours originating from the fibrous connective tissue of the chest wall [8]: they can be intrafascial, intramuscular, and, less frequently, subcutaneous.

They generally have regular contours, with a molten form and intermediate echogenicity (Fig. 7.12).

7.3.6 Desmoids

Deep, extra-abdominal fibromatosis (desmoids) generally affect the dorsal chest wall, shoulder, or thigh.

They are lesions which originate from muscular aponeurosis with intrafascial growth, oval or fusiform in general, with well-defined contours and hypoechoic and inhomogeneous ultrasound structures (Fig. 7.13a–c).

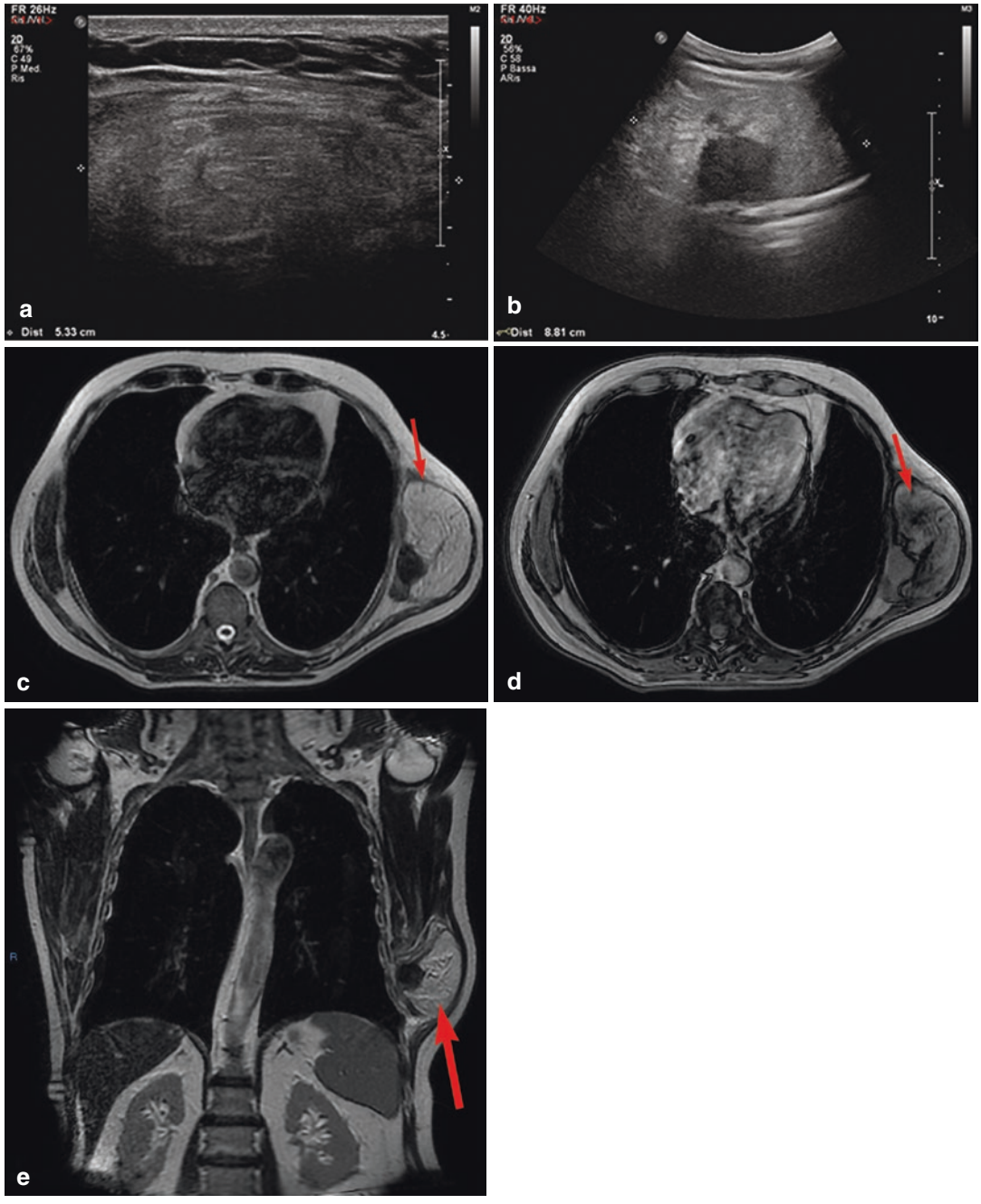

Fig. 7.10 Fibrolipoma of the left serratus anterior muscle. The TUS (**a**, **b**) focused on the voluminous palpable tumefaction and documented the presence of a coarse solid subfascial formation, of about 10 cm, with a nonhomogeneous echostructure, mainly hyperechogenic, with a central hypoechogenic area. MRI (**c**–**e**) confirmed the predominantly adipose nature of the lesion. Histological diagnosis of the atypical fibrolipomatous tumour was posed

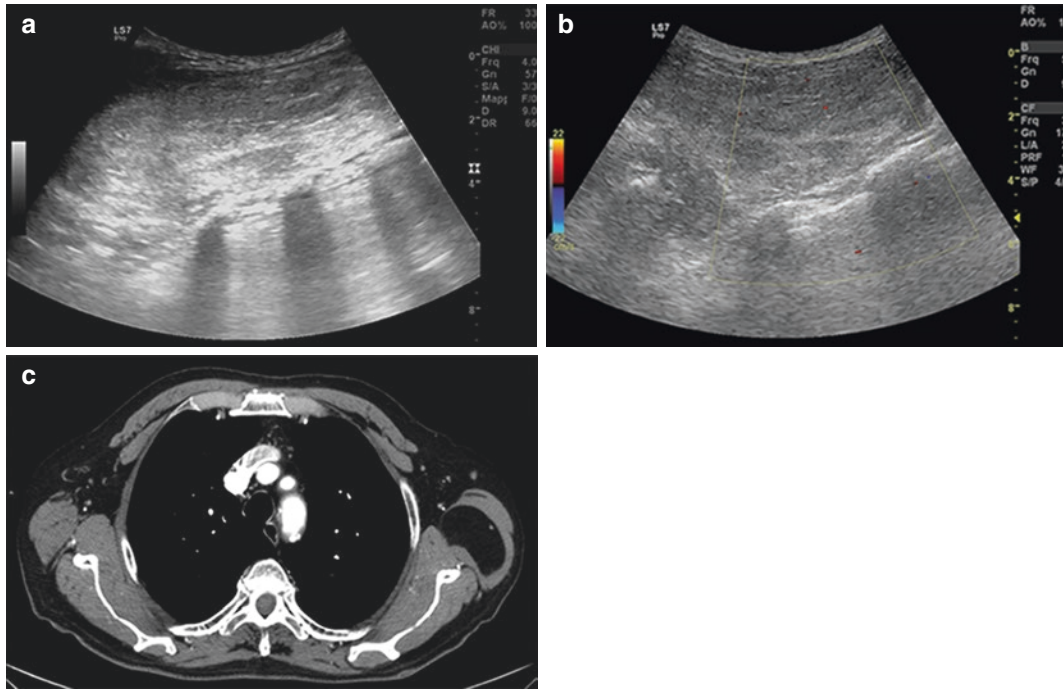

Fig. 7.11 Ultrasound (**a**, **b**) and CT (**c**) of coarse lipoma in the context of the left latissimus dorsi muscle. The colour-Doppler (**b**) showed no vascular signals. The CT confirmed uniform adipose density of the lesion

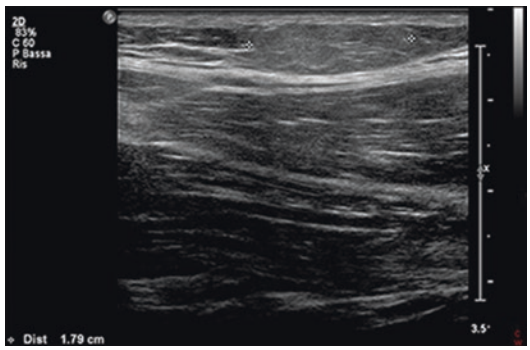

Fig. 7.12 Fibrolipoma. Typical appearance with regular contours and slightly hyperechogenic compared to muscle tissues

These lesions have a variable clinical course; they are generally locally aggressive and often reoccur if they are not removed with wide surgical margins.

7.3.7 Lymphangioma

Lymphangiomas are malformations of the lymphatic vessels, preferentially localized in the head and neck but also found in the mediastinum and axilla.

They can either be directly located or extend to the chest wall.

Under ultrasound examination, they appear as smooth (Fig. 7.14), micro- or macrocyst (i.e., hygroma, cystic) formations, uni- or multilocular.

7.3.8 Epidermal Inclusion Cyst

Epidermal inclusion cysts are localized in the thickness of the skin and the subcutaneous tissue.

They depend on the accumulation of secretive products within the sebaceous glands, for example, as a result of the occlusion of their excretory ducts.

They appear as round cysts with homogeneous hypoechoic content, although sometimes they may exhibit some hyperechogenic spots in the context, caused by the crystallization of sebaceous material.

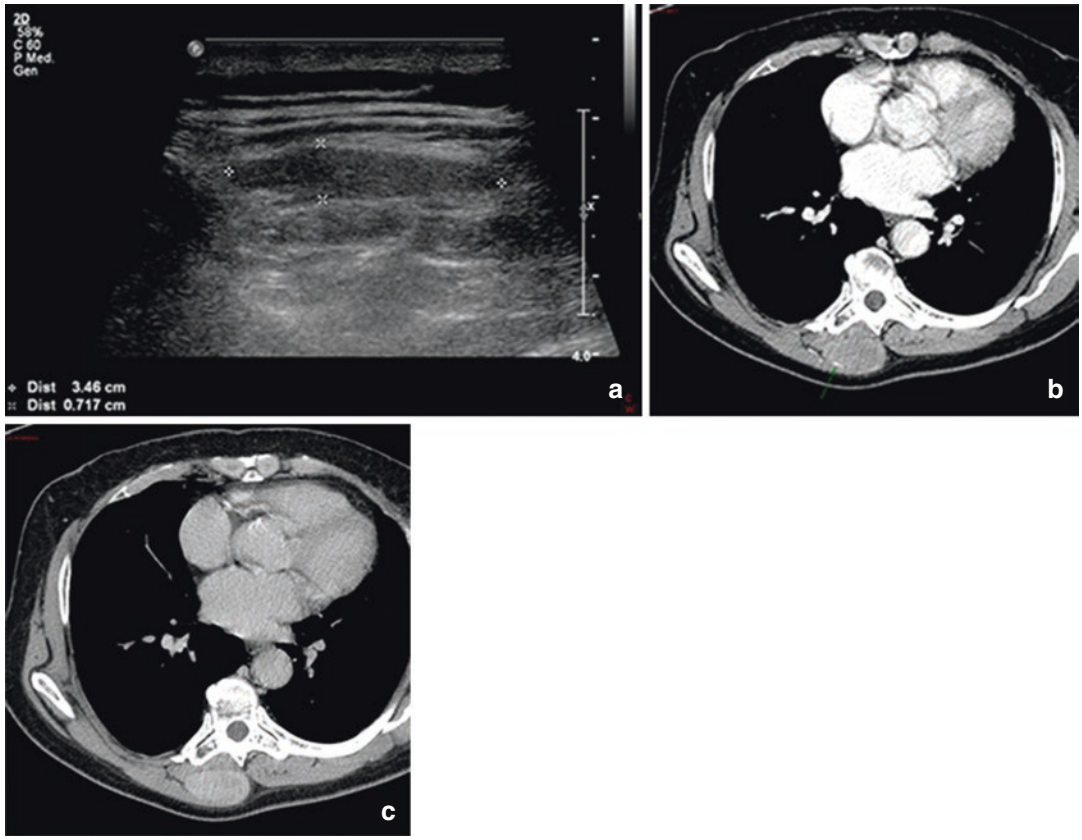

Fig. 7.13 Desmoid thoracic wall. Tumefaction of the back, in the paramedian area, with an ultrasound appearance (**a**) of an elongated subfascial lesion, hypoechogenic with regular contours, with scarce signals at colour Doppler imaging. With a CT (**b**, **c**), the lesion showed a peripheral neoformed vessel in the arterial phase and a homogeneous densitometric increase in the venous phase

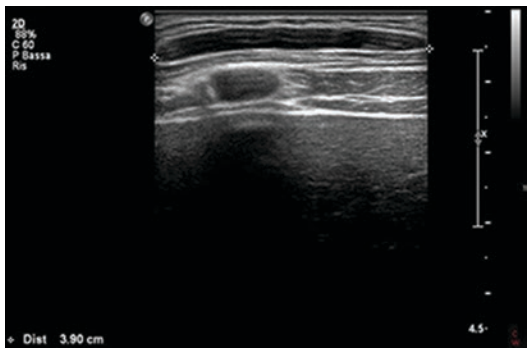

Fig. 7.14 Lymphangioma. An 8-year-old patient. Soft tumefaction. Elongated anechogenic formation with a smooth and thin wall, easily compressible above the costal muscular plane

7.3.9 Elastofibroma

Elastofibroma dorsi is a pseudotumoral lesion, often bilateral, which affects the posterolateral portion of the chest wall, between the apex of the scapula the latissimus dorsi and rhomboid.

It is composed of adipose and fibroelastic tissue, and it is common in subjects engaged in manual occupations, leading to the assumption of a possible reactive genesis as an expression of repeated rubbing movements of the lower angle of the scapula on the adjacent structures.

It is common in older people and females.

Generally, it has semilunar morphology, is located below the muscle plane, and has variable echogenicity depending on the percentage of fatty components (Fig. 7.15a–c).

It features typical hypoechoic or circular internal bands, arranged obliquely in relation to the skin surface and related to the fibroelastic component.

Its typical location, its appearance in TUS, and its possible bilaterality orient the diagnosis [9].

7.3.10 Hemangioma

Hemangiomas are benign vascular tumours and can, although rarely, affect the chest wall [10, 11].

TUS most often reveals them as complex, spongy masses characterized by multiple convoluted vascular spaces [10] (Fig. 7.16a, b).

Angiomas may sometimes simulate a cyst presenting itself as a single cavity with anechoic

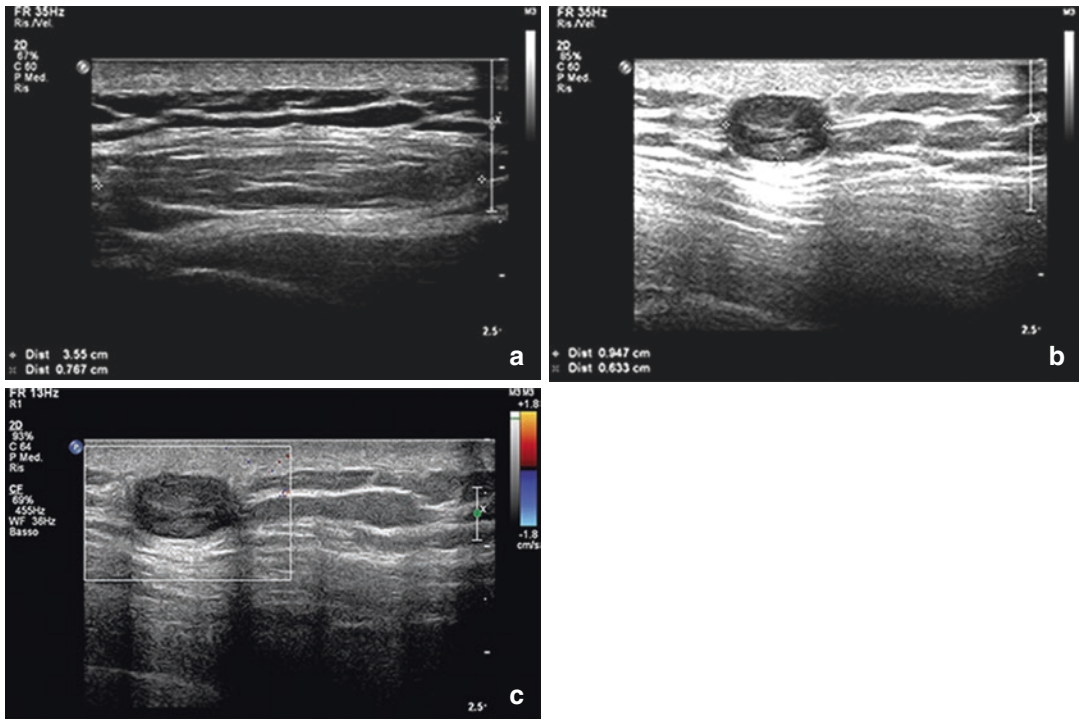

Fig. 7.15 Elastofibroma dorsi. The patient was a young man dedicated to manual activities. The TUS (**a–c**) revealed an elongated, semilunar formation, with a diameter of 3.5 cm in the subcutaneous tissue of the right dorsal thoracic wall, below the scapular apex. The almost isoechogenic formation of the muscle showed a typical longitudinal striation, regular contours, and the absence of vascular signals at colour Doppler imaging

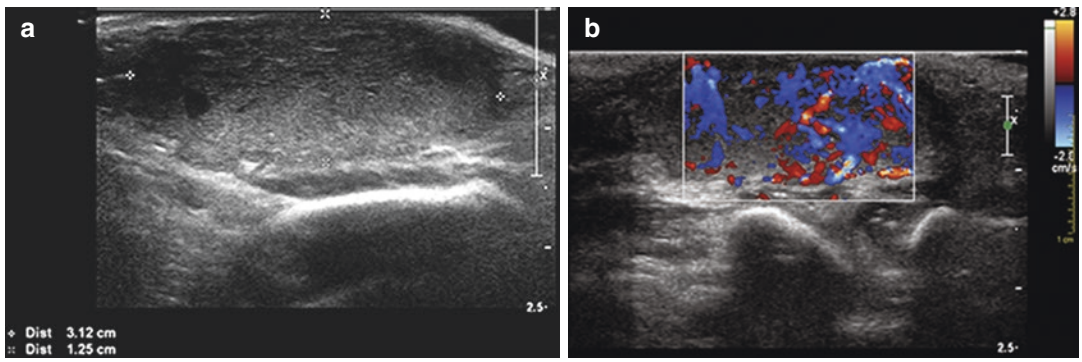

Fig. 7.16 Semilunar angioma in newborn. Formation in the subcutaneous, resting on the underlying muscular fascia with a diameter of about 3 cm, hyperechogenic (**a**) and intensely vascularized with afferent and efferent vessels (**b**)

content. Sometimes, however, multiple septa give the lesion a hyperechogenic appearance similar to that of a solid lesion.

The colour-Doppler shows the vascular signal in dilated vessels, and the flow may be arterial or venous (Fig. 7.17a–c).

7.3.11 Myositis Ossificans

Although rare in this anatomical region, myositis ossificans should be considered in the differential diagnosis of the thoracic wall and thoracic pain masses [12].

It is a metaplastic bone proliferation that develops in the context of the skeletal muscle and sometimes in subcutaneous layers (Fig. 7.18).

Generally, it follows a traumatic event, although there are non-traumatic forms, and the affected area, in the beginning, appears tumulus and sore.

Ossification occurs within a few weeks on the periphery of a fibroblast-like lesion [13], and in TUS, it produces typical acoustic absorption and is therefore easily recognizable.

Therefore, TUS is essential for early diagnosis of the disease when calcifications may not yet be visible on a plain chest X-ray [12].

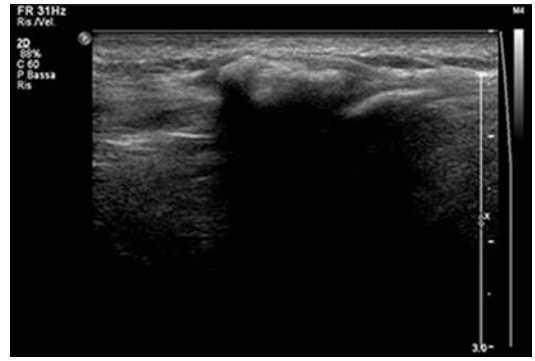

Fig. 7.18 Myositis ossificans. Typical hyper-reflective appearance with rear acoustic barrier due to previous trauma

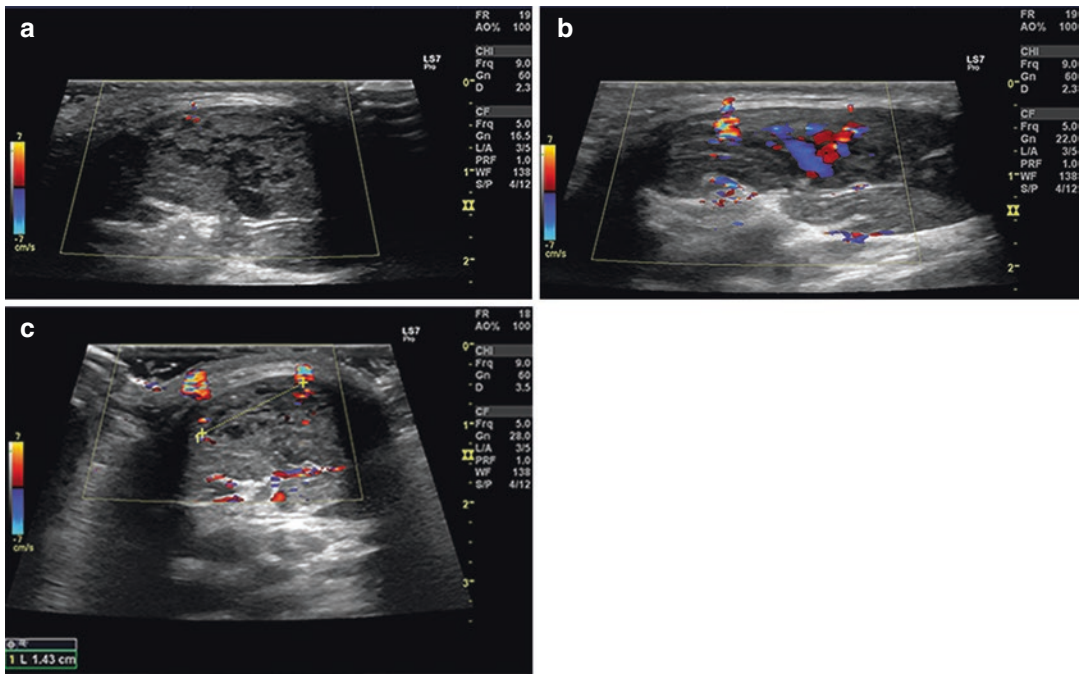

Fig. 7.17 Muscular angiomyolipoma. Ultrasound aspects (**a–c**). Dishomogeneous echostructure formation (vascular, adipose, and muscular components) showing marked vascularization in Doppler colour

7.3.12 Neurogenic Tumours

The neurogenic tumours originate from the spinal nerve roots or the intercostal nerves.

Neurogenic tumours generally appear as regular, hypoechoic, and often with back wall reinforcement formations.

In some cases, TUS can document the continuity of the lesion with the source nerve: the tumour tissue subverts the typical fascicular collated nerve structure.

7.3.13 Primary Malignant Tumours

Primary malignant tumours of the chest wall are mainly sarcomas (chondrosarcomas, osteosarcomas, and Ewing sarcoma family of tumours), plasma cell neoplasms (multiple myeloma and plasmacytoma), and malignant peripheral nerve sheath tumours [14].

Sarcomas of the chest are rare and generally originate from the chest wall tissues, while the primary sarcomas of the pleura are rare.

Generally, sarcomas are bulky lesions with uneven edges and are markedly inhomogeneous due to the coexistence of prominent sects and nodules, an expression of the aberrant proliferation of mesenchymal tissues, fibrous hyperechogenic tissue, and hypo- or anechogenic necrotic regions.

In colour-Doppler, they often appear hyper vascularized with neoformed vessels.

Dynamic TUS can show tumour fixity to deeper structures [8] before and after muscle contraction.

Moreover, ultrasound study allows the evaluation of possible infiltration of bone tissue, which appears with irregularities and cortical interruption.

Ultrasound can ultimately guide biopsy maneuvers for histological characterization. The rib cage is often involved in *multiple myeloma* [15] (Fig. 7.19a–g).

Malignant peripheral nerve sheath tumour is associated with neurofibromatosis type 1, and the transformation of a benign neurofibroma (Fig. 7.20a–c) should be suspected when a patient with neurofibromatosis type 1 is experiencing pain [14].

7.3.14 Lymph Nodes

Ultrasound examination of pectoral, axillary, and laterocervical lymph node assessments exceeds the accuracy of clinical examination [16].

High-frequency linear probes (7.5–12 MHz) are used for the study of surface lymph nodes.

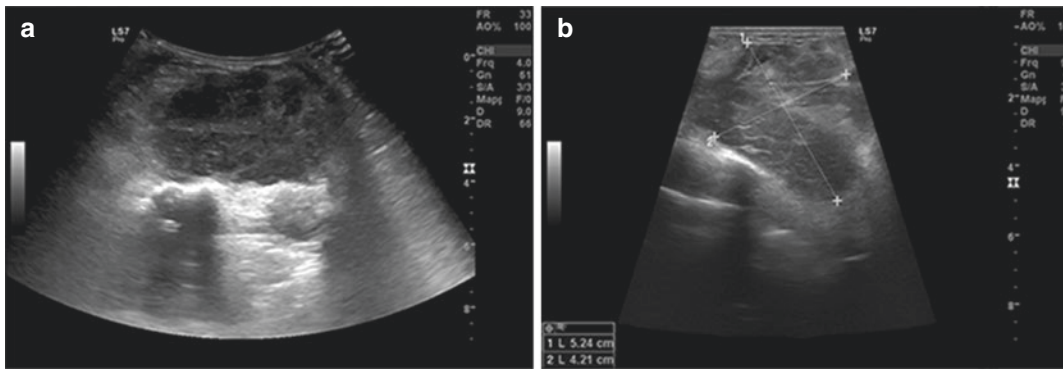

Fig. 7.19 Infiltrating heteroplasia of the thoracic wall in an 82-year-old male patient. The TUS showed a coarse, parasternal lesion of about 5 cm in the chest wall with uneven echostructure, hypo-anechogenic areas (**a**, **b**), and vascular signals in Doppler colour (**c**). Note the irregularity of the underlying bone surface. An X-ray, in LL projection, showed osteolysis of the sternum body (**d**, arrow). This aspect was confirmed by CT (**e**, **f**), which also highlighted the infiltration of surrounding muscular structures. An echo-guided biopsy (**g**) allowed the identification of the expansive lesion, resulting in the diagnosis of multiple myeloma

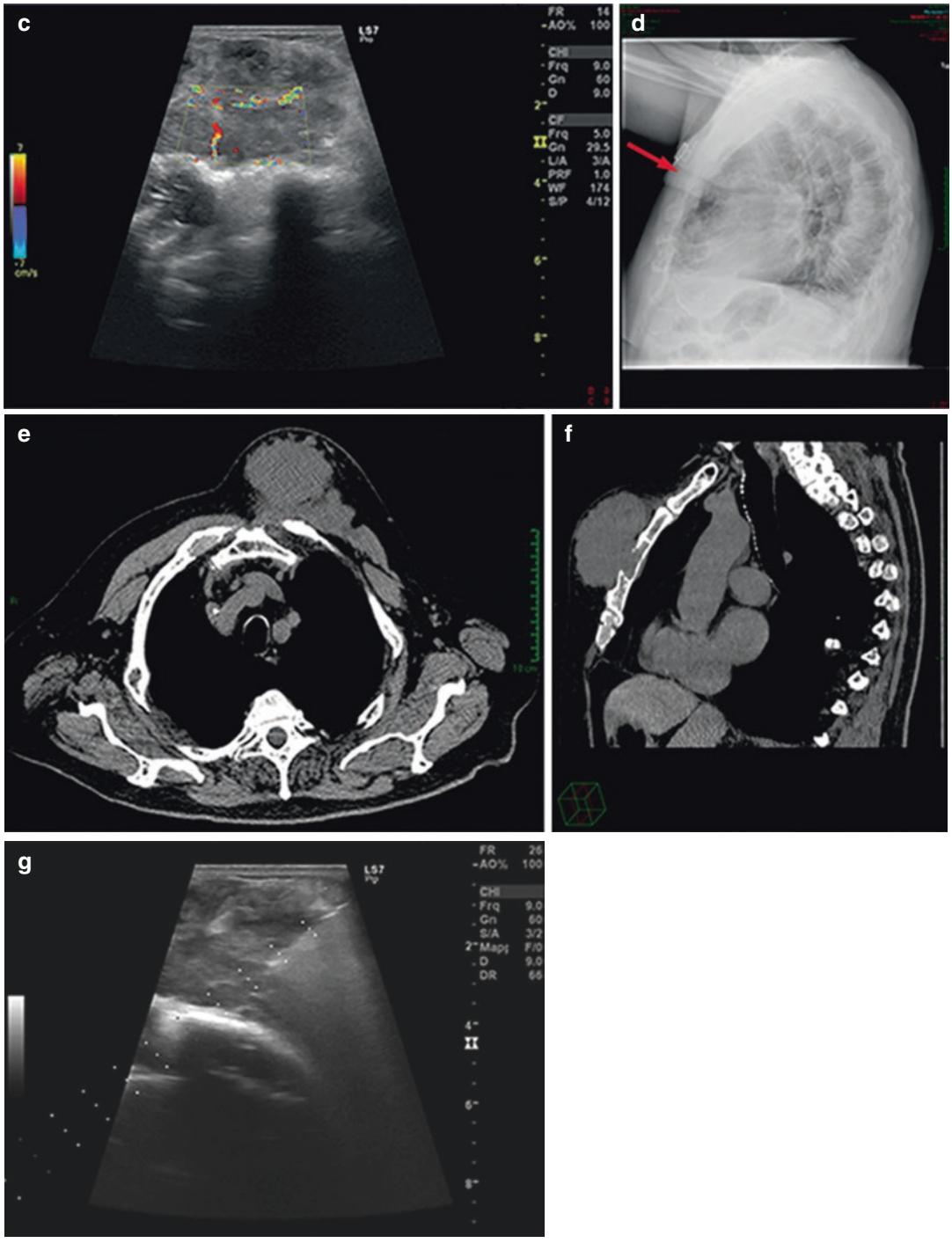

Fig. 7.19 (continued)

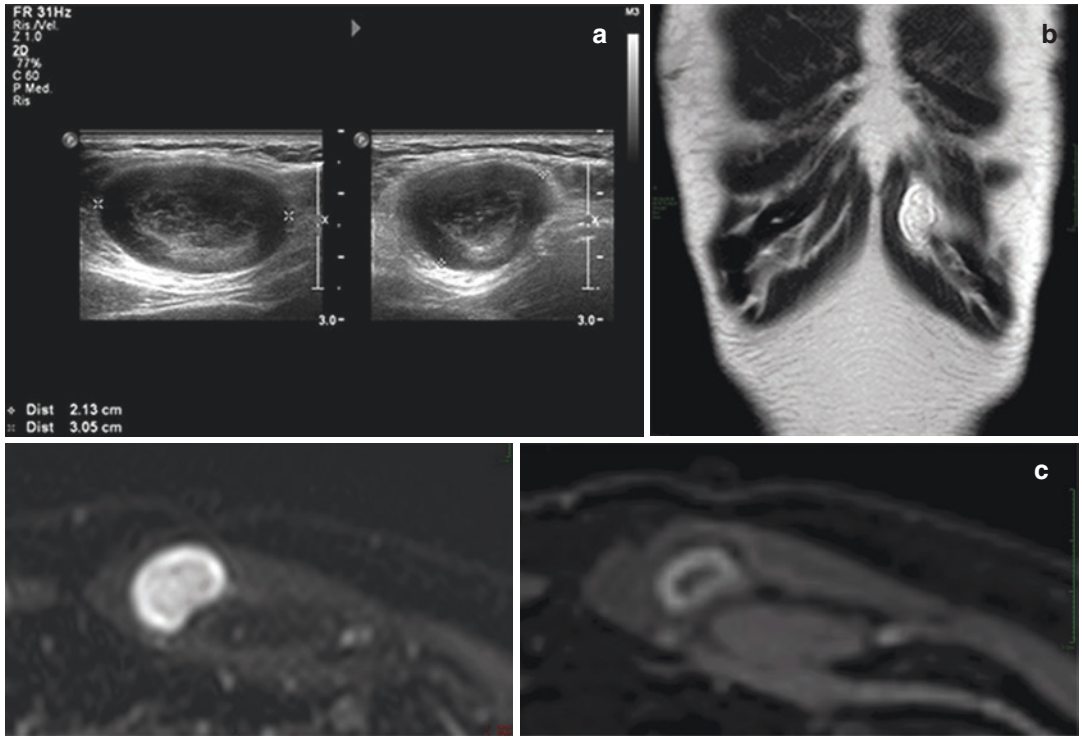

Fig. 7.20 Parasternal neurofibroma in neurofibromatosis. With an ultrasound, the palpable swelling of the thoracic wall showed an oval, unevenly hypoechogenic lesion with regular contours of 2.2 × 3.4 cm (**a**). MRI: Coronal acquisition T2w (**b**); axial acquisition T2w SPAIR(**c**); axial after administration of gadolinium (**d**). With an MRI, the lesion showed low signal in T1w sequences and was hyper intensive in T2w (**b, c**). After administration of contrast medium, enhancement was mainly peripheral (**d**)

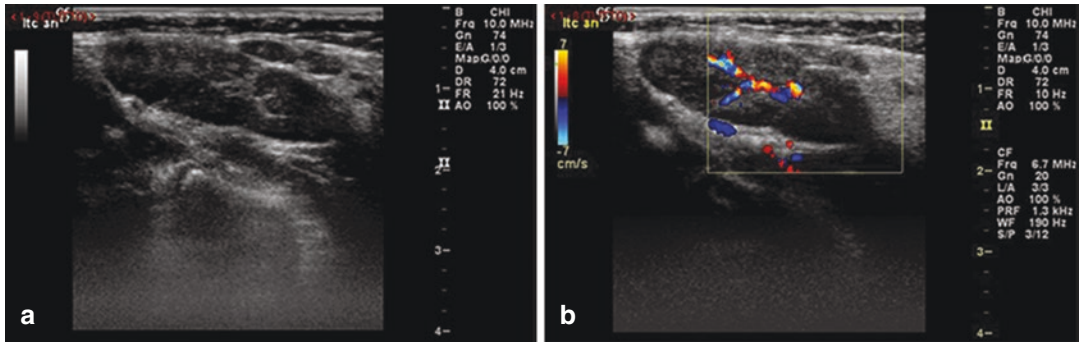

Fig. 7.21 Ultrasound of reactive normal lymph node (**a**), oval-shaped, with hyperechogenic hilum and regular Doppler vascular pattern (**b**)

The normal lymph node has a homogeneously hypoechogenic cortical area [17] and a central or eccentric, hyperechogenic, oval, or linear component.

This second echostructural element depends on the lymphatic sinus interfaces that converge toward the bone marrow and represents an essential sign of normality [17].

In the normal lymph node, with colour- and power-Doppler, only tiny, predominantly central components are seen; they generally have a radial distribution around the central hyperechogenic component [18, 19] (Fig. 7.21a, b).

The *roundness index* (RI) is the ratio between the longitudinal diameter and the transverse lymph node diameter; an oval shape (RI > 1)

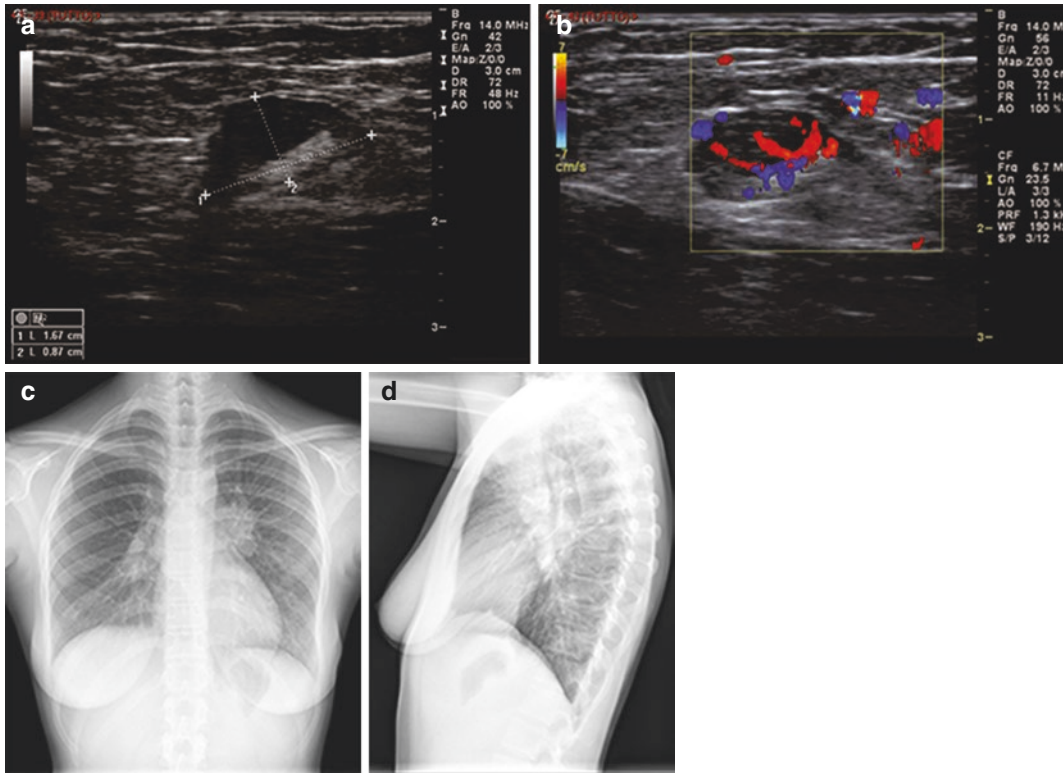

Fig. 7.22 Ultrasound of axillary lymph node in a young patient with non-Hodgkin's lymphoma (**a**, **b**). Evident roundish morphology and vascularization accentuated and altered in Doppler colour. In X-ray examination (**c**, **d**), the enlargement of the pulmonary hila linked to the lymphadenopathic padding is highlighted

orientates toward a reactive nature; vice versa a rounded morphology is indicative of neoplastic involvement (Fig. 7.22a–d).

The roundness index and the central hyperechogenic component [20] represent the most reliable ultrasound parameters to distinguish reactive lymphoma from neoplastic ones.

Focal hypoechoic necrosis areas are typically present in non-Hodgkin's centrocytic or centroblastic type lymphomas and metastases but may also be present in tuberculous lymphadenitis [17, 21].

The ultrasound appearance of neoplastic lymph nodes is unspecific (Fig. 7.23a–d); however, those involved in lymphoproliferative and secondary malignant diseases are often hypoechoic, while metastatic lymph nodes in epithelial neoplasms tend to be more echogenic and inhomogeneous. Nonetheless, the absence of the central echogenic zone is not always synonymous with neoplastic lymph node because it may also depend on the widespread infiltration of fat present in infectious outcomes [22]; in these cases, sometimes fibrotic or macrocalcifications that appear echographically as streaks or hyperechogenic spots are present.

Lymph node microcalcifications are common (65–70% of cases) in the lymph node metastases of medullary and papillary thyroid cancer that mainly affect the cervical, pre-tracheal, and paratracheal lymph nodes [23].

The typical vascular pattern of lymph nodes remains unaltered in hyperplastic-reactive lymph nodes, while it is disrupted in malignant lymphadenopathies, both in the displacement and incarceration of vessels by neoplastic infiltration and neoangiogenic processes [19].

In malignant or tuberculous lymphadenopathies, the colour-Doppler can show eccentric and asymmetric hilar vascularization, and peripheral linear or multifocal flow signals with loss of normal radial distribution or even the absence of vascularization [18, 19].

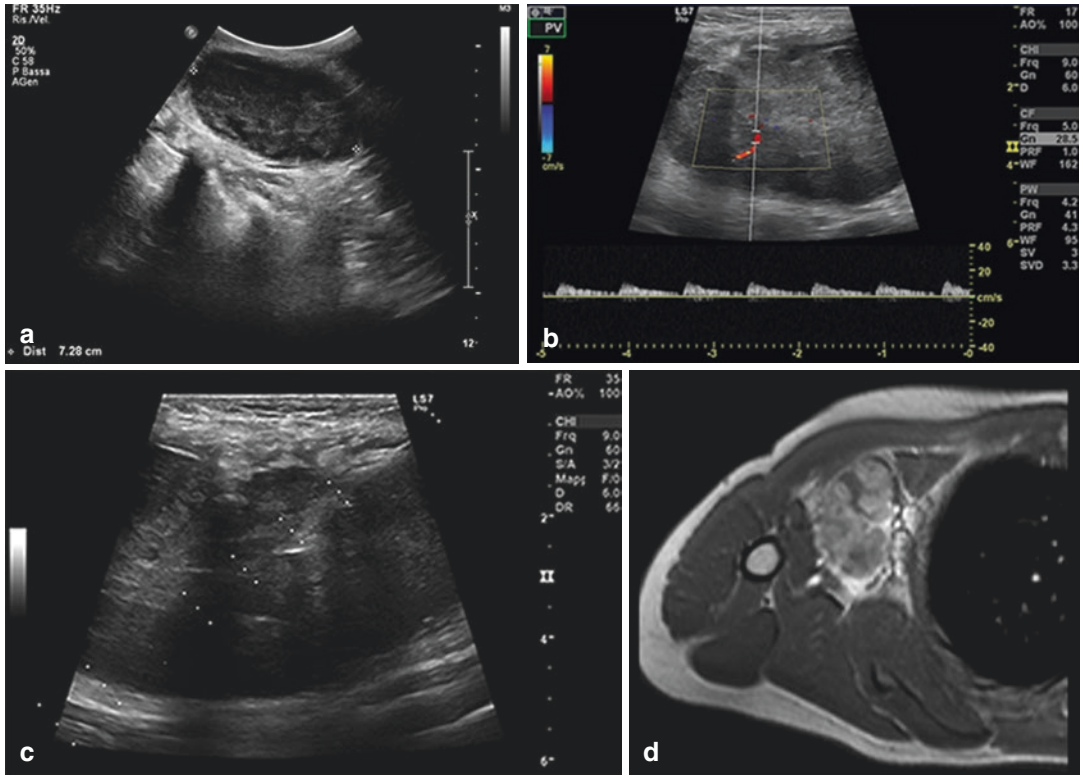

Fig. 7.23 Metastases of the chest wall. TUS with convex probe (**a**), linear probe with Doppler colour (**b**), echo-guided biopsy (**c**), and MRI (**d**): T1W axial image after administration of contrast medium. Solid oval formation of soft tissues (max. diameter 8 cm) with an uneven echostructure, fairly regular contours, and some arterial vessels visible with Doppler. Diagnosis of axillary lymph node metastases from melanoma with unknown origins in a 40-year-old patient

However, any result of a peripheral or mixed vascular pattern—i.e., both central and peripheral—suggests the neoplastic nature of lymphadenopathy [24].

7.3.15 Axillary Lymphadenopathies in Breast Cancer

The ultrasound study of the breast is beyond the scope of this discussion. However, it is advisable to recall the classification of axillary lymph nodes and the role of TUS in patients with breast cancer.

Axillary lymph nodes are classified in three levels based on anatomic relationships with small pectoral muscle.

Lymph nodes placed below the inferior margin of the said muscle belong to level I; those posterior or between the lateral and medial muscle margins are classified as level II; and those medially placed at the upper edge of the muscle, including intravascular lymph nodes, belong to level III.

The ultrasonic probe study is useful in the study of non-palpable lymph nodes at the lower level and the study of palpable lymph nodes of all levels [25].

7.3.16 Supraclavicular Lymphadenopathies

Over the last 20 years, the superiority of noninvasive imaging methods such as TUS and CT compared to palpation evaluation in the detection of overlapping lymph node metastases has been established [26].

To study overlapping lymph nodes with TUS, starting from the base of the neck, one must move

sideways with both transverse and longitudinal scans, extending the study by about 4 cm above the clavicle head [27].

In patients with lung cancer, there are often (41–51% of cases) non-palpable metastatic lymph nodes [28] visible ultrasonically, and TUS has higher accuracy, sensitivity, and specificity than contrast-enhanced CT for primary supraclavicular lymph node metastases in lung cancer [29].

Supraclavicular occult metastases are present in 30% of patients with uterine cervical cancer involving abdominal para-aortic lymph nodes and in 15% of patients with oesophagus carcinoma but may also be present in breast cancer, gastric cancer, pancreas adenocarcinoma, and prostate cancer [30].

Finally, the US-guided FNA of supraclavicular adenopathy is a safe and straightforward tool for diagnosing and staging metastatic lymph nodes in the lung [16] and oesophagal cancer [31] and can also confirm the diagnosis in patients suspected of sarcoidosis [31].

7.3.17 Metastases and Neoplastic Invasion

In lung cancer, TUS with colour-Doppler can evaluate thoracic wall invasion with sensitivity and specificity superior to CT, complementing CT or MRI for preoperative staging [32] and being useful in operational planning [33] (Fig. 7.24a–g).

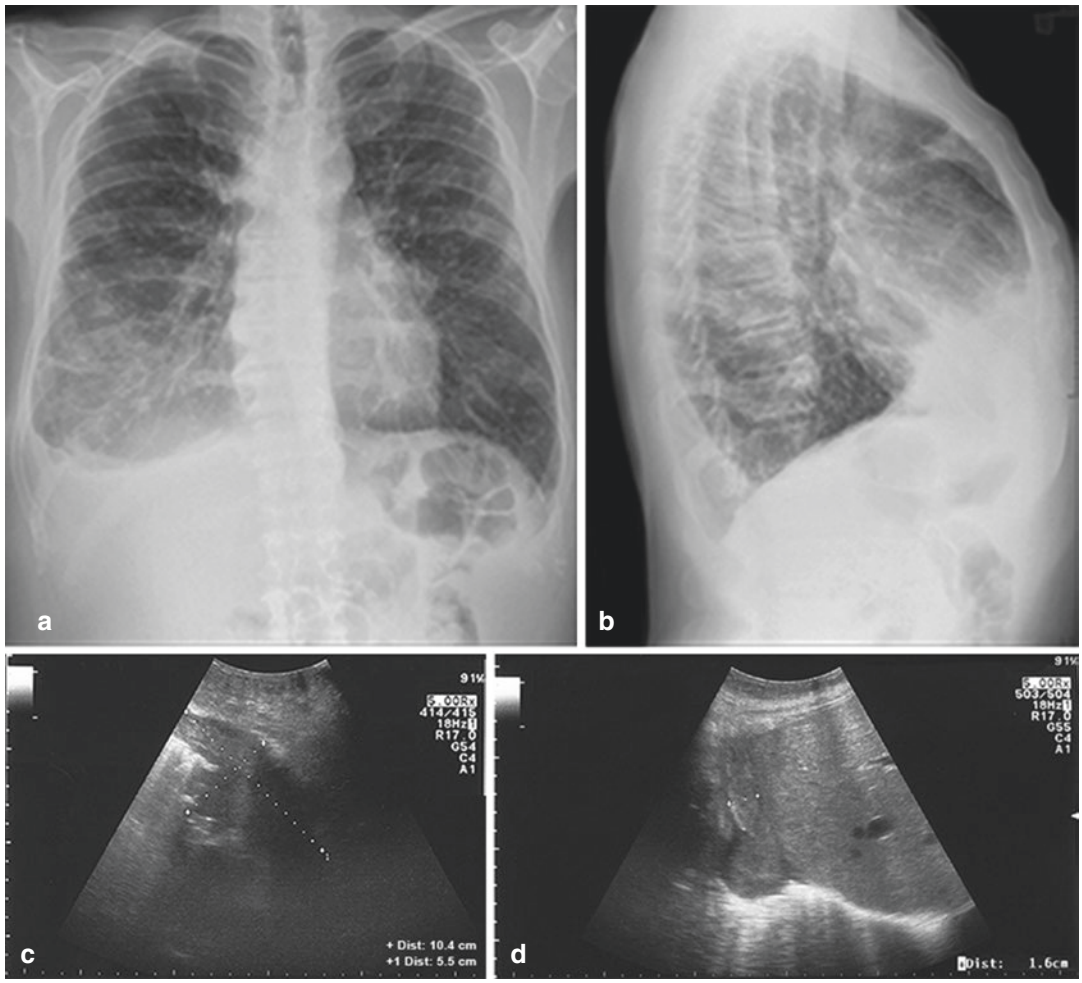

Fig. 7.24 Pulmonary neoplasia infiltrating the chest wall and the diaphragm. X-rays (**a**, **b**); TUS with convex probe (**c**, **d**) and detail of the chest wall with linear probe (**e**); CT (**f**, **g**). The infiltration of the thoracic wall and diaphragm was evident at the TUS, while the CT was more effective in determining the extension of the pathology

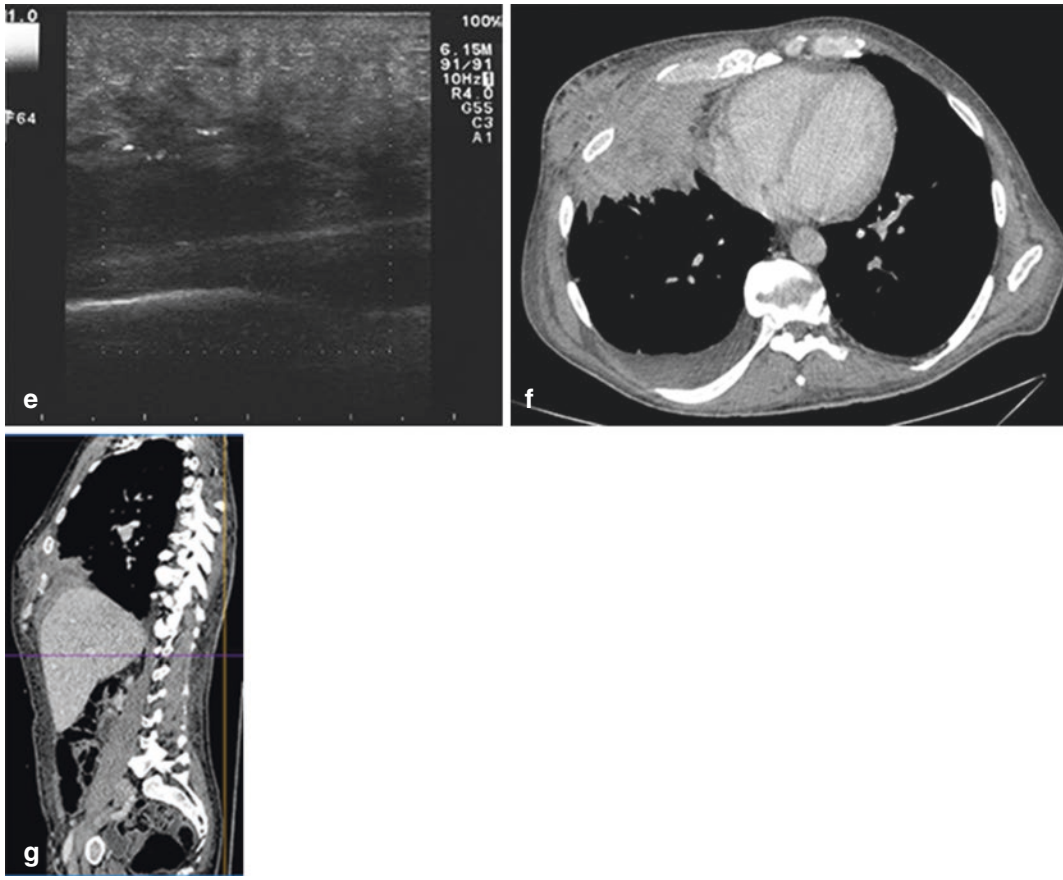

Fig. 7.24 (continued)

Hodgkin's lymphoma sometimes (6.4% of cases) involves the chest wall as the initial or secondary location [34].

The thoracic wall is most often reached by contiguity from an early mediastinal localization in advanced stages of the disease [35] frequently involving the chest skeleton. Instead, recurrences are frequent in the internal lymphatic chain because it is usually excluded from the fields of radiotherapy [36].

On the contrary, non-Hodgkin lymphomas in the chest appear as isolated chest masses, usually in locations that are difficult for ultrasound examination: mediastinal, paratracheal, hernia, and pericardial sites [34, 36].

Finally, soft tissues of the chest wall may sometimes be affected by hematogenic metastases of various malignant neoplasms.

7.3.18 Parietal Emphysema

Overall, parietal emphysema creates an acoustic barrier with the consequent formation of *dirty* acoustic shadows, making it impossible to study the underlying structures and often limiting the visibility of the ribs.

In particular, air causes reverberation artefacts that are classified as E lines and W lines [37] depending on the depth they originate from (Fig. 7.25a, b).

Specifically, E lines are generated at the same depth as the air trapped in a single tissue plane, while W lines are produced at various depths by aerial bubbles scattered between different tissue planes.

Sonographers must learn to recognize tissue emphysema in order to avoid gross interpretative errors.

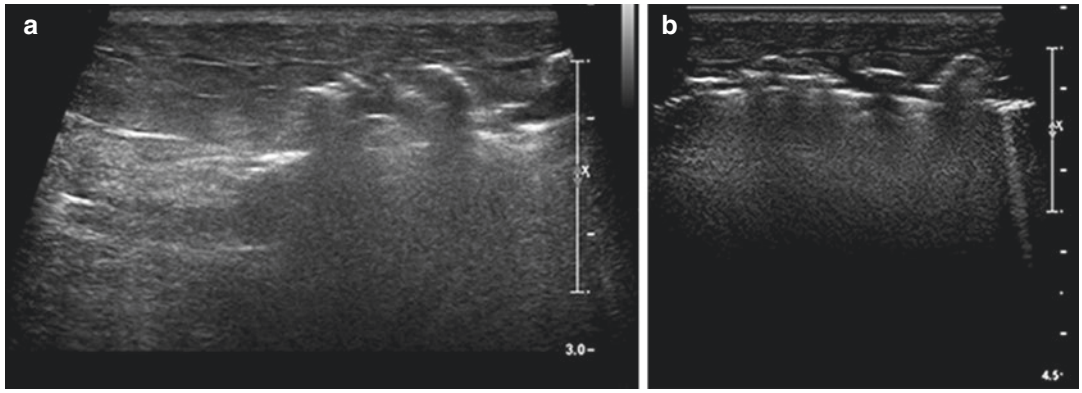

Fig. 7.25 Parietal emphysema (**a, b**). Partial posterior acoustic damming, caused by the presence of air bubbles in the soft tissues of the chest wall

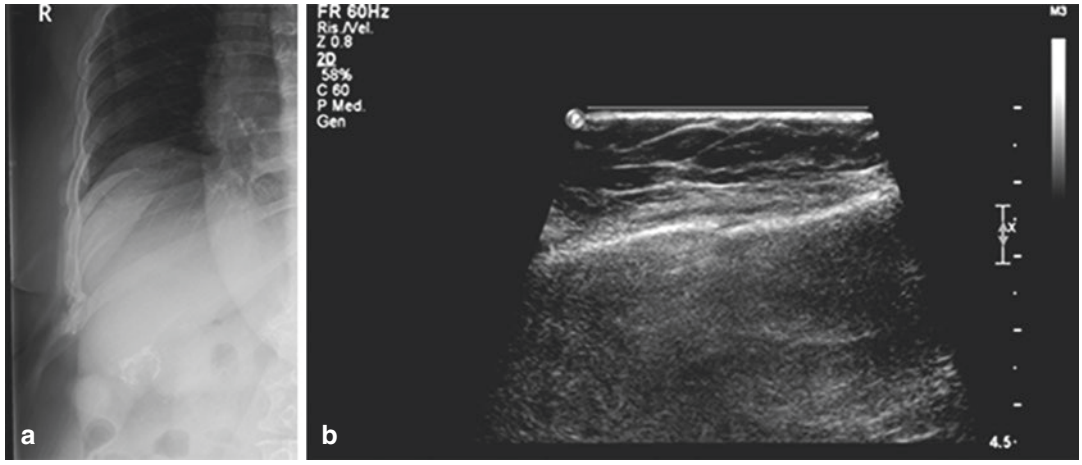

Fig. 7.26 Uncertain cortical irregularity in X-ray examination (**a**) of the eighth right rib at middle axillary, promptly confirmed by the visualization of the cortical bone interrupted in ultrasound examination (**b**)

In particular, E lines and W lines must be distinguished from B lines for their different diagnostic meaning; both E and W lines are formed in soft chest wall tissues, are fixed, and prevent the ribs from appearing, while B lines are generated at the pleural line level and are modified with respiratory acts.

The presence of B lines excludes pneumothorax. Instead, E and W lines indicate the presence of subcutaneous emphysema, a condition often associated with pneumothorax [38].

If the parietal emphysema is not too widespread, one can attempt to create acoustic access to the underlying structures by applying moderate pressure to the transducer, using ribs as fixed points to squeeze and shift the air bubbles.

7.4 Pathology of Scheletric Components

7.4.1 Fractures

The radiological diagnosis of bone fractures in the chest is not always easy, particularly if the radiogram is performed immediately after trauma and in the case of undisplaced fractures.

TUS allows for the identification of twice the amount of rib fractures compared to the standard chest radiogram performed with specific projections [39] (Fig. 7.26a, b).

It can also detect associated conditions such as pleural effusion, pneumothorax, pulmonary contusions, and chest wall haemorrhages [40].

In costal, cranial, and scapular fractures, TUS allows direct visualization of the interruption of the bone cortical, any fragments, and, if the fracture is disintegrated, the uneven levels of the fracture stumps (Fig. 7.27a–c).

The *lighthouse phenomenon*, also called *chimney phenomenon*, consists of reverberation echoes extending from the margin of the fracture to the bottom [40, 41].

This sign can be summoned by exerting minimal pressure at the point where the patient reports pain [42] and can be the only visible echographic sign in composite fractures.

To precisely locate sternal fractures, it is useful to refer to the joints between the manubrium, the sternal body, and the xiphoid process.

Fractures of the chest cage can form hematomas of variable size.

In the beginning, hematoma appears hypoanechoic, while about two weeks after the trauma, an increasing number of echoes and small acoustic shadows appear. They are signs of the repairing processes, and the first calcifications [40].

After consolidation, a more or less evident hump can remain in the bone profile [40, 43] (Fig. 7.28a, b).

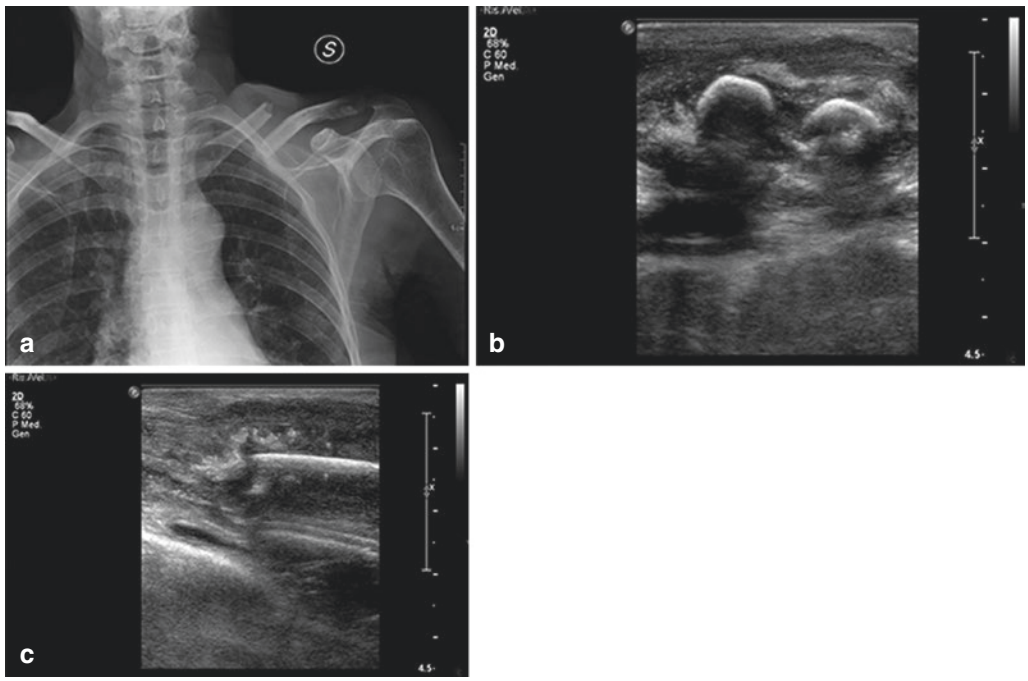

Fig. 7.27 Fracture at the middle third of the left collarbone. X-ray (**a**) and ultrasound (**b**, **c**)

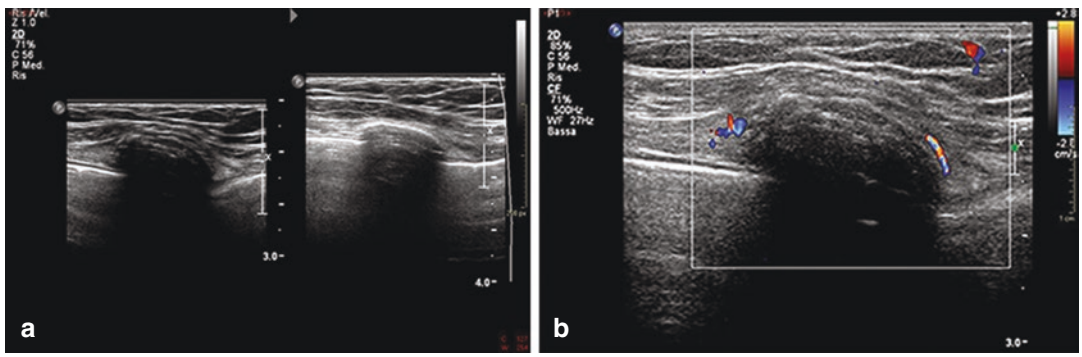

Fig. 7.28 Healing of a rib fracture. Ultrasound (**a**, **b**) of a fibrocartilaginous callus at the anterior end of the second right rib in a young woman

7.4.2 Osteomyelitis

Clinical diagnosis of osteomyelitis, cellulite, and abscess of soft chest wall tissues is challenging.

In osteomyelitis, inflammation related to bone necrosis and ischemic phenomena in the microcirculation produces an exudate that emerges from the cortical bone, forming fluid collections [44], which may sometimes contain a gaseous component or, in tuberculous forms, minute calcifications [45].

Fluid collections caused by osteomyelitis are located directly on the bone surface, while fluids originating from soft tissues (i.e., cellulite, lymphedema, abscess, or hematoma) remain separate from the cortical bone because the soft tissues remain attached to the bone.

Therefore, a fluid collection in direct contact with the bone is a sensitive sign of osteomyelitis and, when associated with the clinical data, allows for diagnosis [44].

However, this is a non-specific sign since fluid collections in direct contact with cortical bone can also be small hemorrhagic outbreaks in the presence of costal metastases [45].

7.4.3 Neoplastic Osteolytic Lesions

The thoracic cage may be home to metastases of several cancers (Fig. 7.29a–f) and in particular bronchogenic cancer, plasmacytoma, and breast, prostate, and kidney tumours.

While osteoblastic injuries do not show up in TUS, most osteolytic metastases can be detected because they reduce bone calcium content and increase ultrasound permeability.

In some cases, a well-conducted ultrasound can even allow the pleura to be seen behind a costal lesion [46].

More commonly, these lesions result in the reduction in sharpness or the disappearance of the back acoustic shadow [46, 47].

Upon examination, the neoplastic tissue component generally looks like a hypoechoic mass, while periosteal edema appears to be a localized thickening of soft tissues.

Ultrasound ultimately provides the guide to bioptic sampling for the characterization of osteolytic lesions of the chest cage [48] (Fig. 7.30a–d).

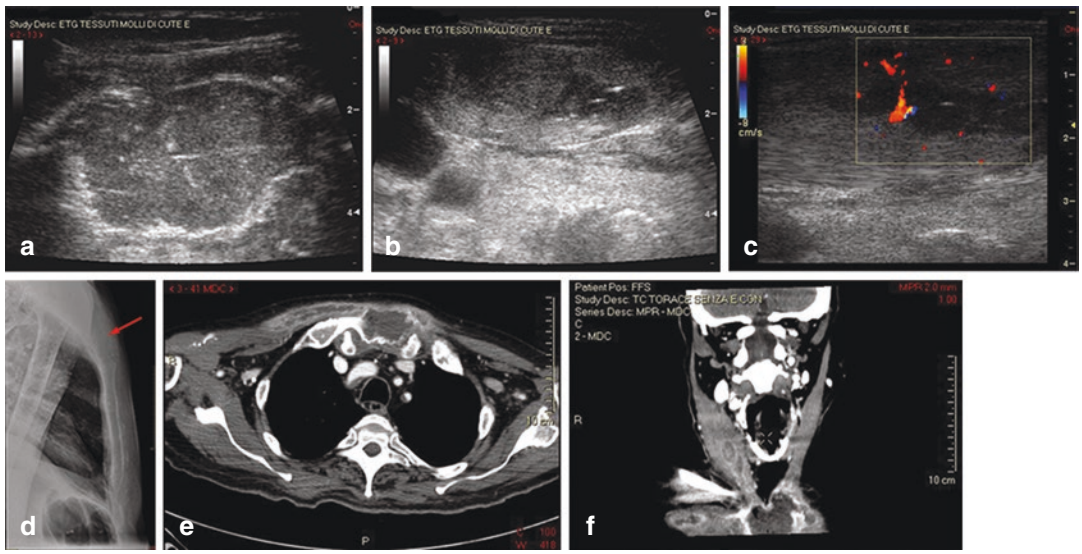

Fig. 7.29 Metastasis within the sternocleidomastoid muscle from colon neoplasm. In correspondence with painful swelling, the TUS showed a solid lesion that interrupted the cortical bone of the sternal manubrium (**a**). Hypoechogenic lesions were present in the sternocleidomastoid muscle, (**b**) with signs of lesion neovascularization in Doppler colour (**c**). An X-ray, in LL projection, confirmed sternal osteolysis (**d**, arrow). The axial scan CT showed the lithic area of the sternal manubrium (**e**). Injuries in the sternocleidomastoid muscle were also visible, better demonstrated in coronal reconstruction (**f**)

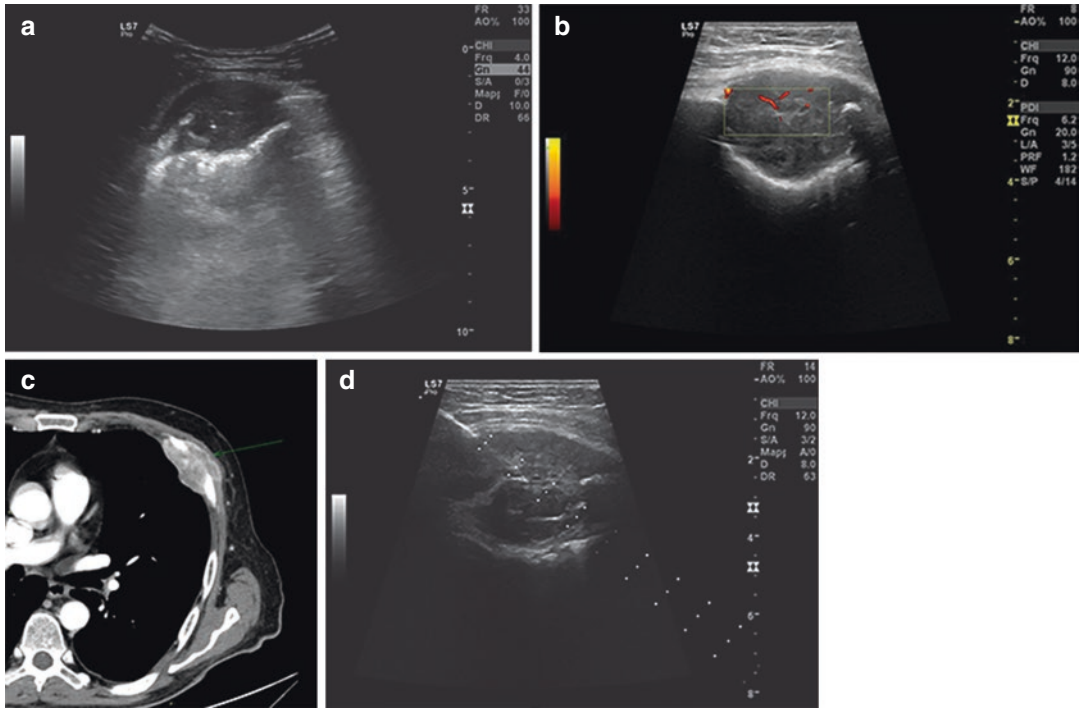

Fig. 7.30 Costal metastases from bladder cancer. The TUS was performed to assess a painful swelling of the anterior-lateral chest wall in the lower third of the left hemithorax. A solid lesion (**a**) interrupted the cortical bone of the mid-anterior arc of cost, with uneven echo-structure and signs of lesion neovascularization in Doppler colour (**b**). Axial CT scan (**c**) confirmed the finding. An echo-guided biopsy (**d**) allowed the identification of the expansive lesion, resulting in the diagnosis of bladder cancer metastases

7.5 Conclusions

Ultrasound study is useful in supporting clinical evaluation and other imaging methods in different diagnostic pathways, both in conditions affecting soft tissues and chest wall skeletal components.

TUS also has purely specialist applications, including an essential role in staging certain cancers, biopsy procedures, and operational planning.

The method is easily available, economical, radiation-free, and easy to execute. There are some limitations however, mainly related to conditions which hinder the correct positioning of the probe or that limit the penetration of the ultrasound beam, as in the case of parietal emphysema.

References

1. Lee RKL, Griffith JF, Ng AWH, Sitt JCM. Sonography of the chest wall: a pictorial essay. J Clin Ultrasound. 2015;43:525–37.
2. Broggio D, Lechaftois X, Abline O, Fleury B, Vial A, Corrèze P, Franck D, Merzoug V. Energy dependent chest wall thickness equations for male lung monitoring with germanium detectors. Health Phys. 2014;106(3):405–14.
3. Aliotta A, Ferraioli G, Livraghi T. Standard per una corretta esecuzione dell'esame ecografico. In: Journal of ultrasound, speciale 2009. XXI Congresso Nazionale SIUMB. Milano: Elsevier; 2009. p. 33–5.
4. Mathis G. Chest sonography. Berlin: Springer; 2008. p. 229.
5. Gardelli G, Feletti F, Nanni A, Mughetti M, Piraccini A, Zompatori M. Chest ultrasonography in the ICU. Respir Care. 2012 May;57(5):773–81.
6. Feletti F, Mucci V, Aliverti A. Chest Ultrasonography in Modern Day Extreme Settings: From Military Setting and Natural Disasters to Space Flights and Extreme Sports. Can Respir J. 2018: 8739704.
7. Cammarota T, et al. Ecografia in dermatologia. Milano: Poletto Editore; 1998. p. 79–93.
8. Athanassiadi K, Kalavrouziotis G, Rondogianni D, Loutsidis A, Hatzimichalis A, Bellenis I. Primary chest wall tumors: early and long-term results of surgical treatment. Eur J Cardiothorac Surg. 2001 May;19(5):589–93.
9. Falidas E, Arvanitis D, Anyfantakis G, et al. Painful elastofibroma dorsi: a report of a case and

a brief review of the literature. Case Rep Orthop. 2013;2013:794247.
10. Tarantino CC, Vercelli A, Canepari E. Angioma of the chest wall: a report of 2 cases. J Ultrasound. 2011;14(1):18–21.
11. Dzian A, Hamzík J. Intercostal hemangioma of the chest wall. Kardiochir Torakochirurgia Pol. 2016;13(1):58–60.
12. Ergun T, Lakadamyali H, Lakadamyali H, Gokay E. Myositis ossificans in the right inferior thoracic wall as an unusual cause of lower thoracic-upper abdominal pain: report of a case. Surg Today. 2008;38(10):962–4.
13. Saussez S, Blaivie C, Lemort M, Chantrain G. Non-traumatic myositis ossificans in the paraspinal muscles. Eur Arch Otorhinolaryngol. 2006;263(4):331–5.
14. Bueno J, Lichtenberger JP 3rd, Rauch G, Carter BW. MR imaging of primary chest wall neoplasms. Top Magn Reson Imaging. 2018;27(2):83–93.
15. Oymak FS, Karaman A, Soyuer I, et al. Pulmonary and chest wall involvement in multiple myeloma. Tuberk Toraks. 2003;51(1):27–32.
16. Tian HY, Xu D, Liu JP, Mao WM, Chen LY, Yang C, Wang LP, Shi KY. Contribution of ultrasound-guided fine-needle aspiration cell blocks of metastatic supraclavicular lymph nodes to the diagnosis of lung cancer. J Cancer Res Ther. 2015;11(Suppl):C234–8.
17. Vassallo P, Wernecke K, Roos N, Peters PE. Differentiation of benign from malignant superficial lymphadenopathy: the role of high-resolution US. Radiology. 1992;183(1):215–20.
18. Na DG, Lim HK, Byun HS, et al. Differential diagnosis of cervical lymphadenopathy: usefulness of color Doppler sonography. AJR Am J Roentgenol. 1997;168(5):1311–6.
19. Wu CH, Chang YL, Hsu WC, et al. Usefulness of Doppler spectral analysis and power Doppler sonography in the differentiation of cervical lymphadenopathies. AJR Am J Roentgenol. 1998;171(2):503–9.
20. Stiglich F, Barbonetti C, Di Lorenzo E, et al. Diagnostic reliability of ultrasonography in the preoperative staging of the N parameter in head and neck neoplasms. Radiol Med. 1991;81(6):838–43.
21. Som PM. Lymph nodes of the neck. Radiology. 1987;165:593–600.
22. Rubaltelli L, Proto E, Salmaso R, et al. Sonography of abnormal lymph nodes in vitro: correlation of sonographic and histologic findings. AJR Am J Roentgenol. 1990;155(6):1241–4.
23. Gorman B, Charboneau JW, James EM, et al. Medullary thyroid carcinoma: role of high resolution US. Radiology. 1987;162:147–50.
24. Dragoni F, Cartoni C, Pescarmona E, et al. The role of high resolution pulsed and color Doppler ultrasound in the differential diagnosis of benign and malignant lymphadenopathy: results of multivariate analysis. Cancer. 1999;85(11):2485–90.
25. Lee SC, Jain PA, Jethwa SC, Tripathy D, Yamashita MW. Radiologist's role in breast cancer staging: providing key information for clinicians. Radiographics. 2014;34(2):330–42.
26. Kendirlinan R, Özkan G, Bayram M, et al. Ultrasound guided fine-needle aspiration biopsy of metastases in nonpalpable supraclavicular lymph nodes in lung cancer patients. Multidiscip Respir Med. 2011;6(4):220–5.
27. van Overhagen H, Brakel K, Mark W, et al. Metastases in supraclavicular lymph nodes in lung cancer: assessment with palpation, US, and CT. Radiology. 2004;232:75–80.
28. Lee DH, Yoon TM, Lee JK, Lim SC. Supraclavicular lymph node excision biopsy in patients with suspected supraclavicular lymph node metastasis of lung cancer: experience in a Tertiary Hospital. Chonnam Med J. 2017;53(1):69–72.
29. Liu Z, Cheng W, Li P, Sun Y, Wang Q. Clinical value of ultrasound in the diagnosis of supraclavicular lymph node metastasis of primary lung cancer. Zhongguo Fei Ai Za Zhi. 2014;17(9):663–8.
30. Fultz PJ, Feins RH, Strang JG. Detection and diagnosis of nonpalpable supraclavicular lymph nodes in lung cancer at CT and US. Radiology. 2002;222(1):245–51.
31. Patrick J, Fultz L, Amy R, et al. Sonographically guided biopsy of supraclavicular lymph nodes: a simple alternative to lung biopsy and other more invasive procedures. AJR. 2003;180:1403–9.
32. Sripathi S, Mahajan A. Comparative study evaluating the role of color Doppler sonography and computed tomography in predicting chest wall invasion by lung tumors. J Ultrasound Med. 2013;32(9):1539–46.
33. Tahiri M, Khereba M, Thiffault V, Ferraro P, Duranceau A, Martin J, Liberman M. Preoperative assessment of chest wall invasion in non-small cell lung cancer using surgeon-performed ultrasound. Ann Thorac Surg. 2014;98(3):984–9.
34. Bae YA, Lee KS. Cross-sectional evaluation of thoracic lymphoma. Radiol Clin N Am. 2008;46:253–64.
35. Guermazi A, Brice P, De Kerviler EE, et al. Extranodal Hodgkin disease: spectrum of disease. Radiographics. 2001;21:161–79.
36. Sharma A, Fidias P, Hayman A, et al. Pattern of lymphoadenopathy in thoracic malignancies. Radiographics. 2004;24:419–39.
37. Lichtenstein D. Lung ultrasound in the critically ill. Berlin: Springer; 2015. p. 105.
38. Lichtenstein D. General ultrasound in the critically ill. Berlin: Springer; 2005. p. 107–13.
39. Bitschnau R, Gehmacher O, Kopf A. Ultrasound diagnosis of rib and sternal fracture. Ultraschall Med. 1997;18:158–61.
40. Paik SH, Chung MJ, Park JS, et al. High-resolution sonography of the rib: can fracture and metastasis be differentiated? AJR. 2005;184:969–74.
41. Beckh S, Bölcskei PL, Lessnau KD. Real-time chest ultrasonography. A comprehensive review for the pulmonologist. Chest. 2002;122:1759–73.

42. Mathis G, Blank W. The chest wall in chest sonography. 2nd ed. Berlin: Springer; 2008. p. 12–22.
43. Dubs-Kunz B. Sonography of chest wall. Eur J Ultrasound. 1996;3:103–11.
44. Abiri MM, Kirpekar R, Ablow RC. Osteomyelitis: detection with US. Radiology. 1997;172:509–11.
45. Park CM, Chung KB, Suh WH. Osteomyelitis: detection with US. Radiology. 1991;178:890a.
46. Sugama Y, Tamaki S, Kitamura S, et al. Ultrasonographic evaluation of pleural and chest wall invasion of lung cancer. Chest. 1998;93:275–9.
47. Vogel B. Ultrasonographic detection and guided biopsy of thoracic osteolysis. Chest. 1993;104(4):1003–5.
48. Targhetta R, Balmes P, Marty-Double C. Ultrasonically guided aspiration biopsy in osteolytic bone lesions of the chest wall. Chest. 1993;103:1403–8.